

**Reducing Dose While Maintaining Image Quality for Cone Beam Computed Tomography**

By

Peter G. Kroening

A thesis submitted in partial fulfillment of the requirements for  
the degree of

Bachelor of Science

Houghton College

May 2012

Signature of Author .....

Department of Physics  
May 30, 2012

.....

Dr. Brian Winey  
Radiation Physicist, Massachusetts General Hospital  
Instructor, Harvard Medical School

.....

Dr. Mark Yuly  
Professor of Physics  
Houghton College

# **Reducing Dose While Maintaining Image Quality for Cone Beam Computed Tomography**

By

Peter G. Kroening

Submitted to the Houghton College Department of Physics  
on May 30, 2012 in partial fulfillment of the requirement for  
the degree of Bachelor of Science

## **Abstract**

Three dimensional volumetric cone beam imaging, or cone beam computed tomography (CBCT), scans were taken of a quality assurance Catphan phantom, human pelvis phantom, and human head phantom at the Department of Radiation Oncology at Massachusetts General Hospital. Preset values of the gantry speed and the pulse current were varied to adjust the dose delivered for CBCT scans. The CBCT images were analyzed for image quality as a function of the dose received by the phantom. Radiation dose was measured with an electrometer for the various preset combinations. If the elapsed time of a scan can be decreased and the pulse current lowered while maintaining adequate image quality, then the average radiation delivered to a patient can be decreased. It was found that the image quality was maintained for faster scans with lower currents such that patients will be exposed to lower dosages.

Thesis Supervisor: Dr. Mark Yuly

Title: Professor of Physics

## TABLE OF CONTENTS

TABLE OF FIGURES .....	5
<b>Chapter 1</b> HISTORY AND MOTIVATION .....	6
1.1 Introduction .....	6
1.2 Early CT Scanning.....	7
1.3 Cone Beam CT.....	8
1.4 Image Quality and Dose.....	9
1.5 CT Images.....	9
<b>Chapter 2</b> THEORY .....	11
2.1 Introduction .....	12
2.2 The Cone Beam .....	12
2.3 Flat Panel Detector .....	13
2.4 Lambert-Beer Law .....	15
2.5 Image Reconstruction .....	18
<b>Chapter 3</b> IMAGE ANALYSIS .....	22
3.1 Introduction .....	23
3.2 Experimental Procedure .....	23
3.3 Image Analysis .....	24
3.3.1 Geometrical Alignment.....	25
3.3.2 Density .....	26
3.3.3 Contrast-to-Noise Ratio .....	26
3.3.4 Image Uniformity.....	27
3.4 Measuring Radiation .....	27
<b>Chapter 4</b> RESULTS AND CONCLUSION .....	29
4.1 Introduction .....	30
4.2 CBCT Image Quality.....	30
4.3 Discussion .....	35
4.4 Future Plans .....	35
<b>Appendix A</b> MATLAB CODE .....	37
A.1 Image Analysis Codes.....	36

A.2	Image Density and CNR.....	36
A.3	Image Uniformity .....	37
A.4	Image Linearity.....	37
Appendix B	TABLE OF MEASUREMENTS .....	39
B.1	Figure 17 Data .....	39
B.2	Figure 18 Data .....	39
B.3	Figure 19 Data .....	40
B.4	Figure 20 Data.....	40
B.5	Figure 21 Data .....	41
REFERENCES	.....	43

## TABLE OF FIGURES

Figure 1. Elekta Synergy CBCT scanner.....	6
Figure 2. CT scanner history .....	8
Figure 3. Catphan phantom.....	10
Figure 4. Catphan section 404 scan slice.....	11
Figure 5. X-ray tube. ....	13
Figure 6. Flat Panel Detector. ....	14
Figure 7. Image Intensifier Detector.....	14
Figure 8. TFT/Photodiode circuit. ....	15
Figure 9. Lambert-Beer Law for homogeneous material of thickness $x$ .....	16
Figure 10. X-ray attenuation plot.....	16
Figure 11. Lambert-Beer Law for inhomogeneous material. ....	17
Figure 12. Beam path reconstruction graph. ....	19
Figure 13. Catphan image alignment.....	24
Figure 14. Pelvis phantom CNR.....	25
Figure 15. Catphan image uniformity. ....	27
Figure 16. CTDI Phantom.....	28
Figure 17. Head and neck image quality plot (Catphan). ....	30
Figure 18. Head and neck uniformity plot (Catphan).....	31
Figure 19. Pelvis image quality (Catphan).....	32
Figure 20. Pelvis image quality (Pelvis Phantom).....	33
Figure 21. Pelvis uniformity plot (Catphan). ....	34

## Chapter 1

### HISTORY AND MOTIVATION

#### 1.1 Introduction

CT is an indispensable tool in the field of radiation oncology [1]. CT imaging is used for rapid patient imaging in surgical suites and radiation oncology treatment rooms. A CT scanner, seen in Figure 1, uses an x-ray source and detector to measure the attenuation of the x-ray photons through a target. The attenuation is used to reconstruct an image of the inside of the target. Being able to visualize the inside of a human being is significant in medicine because it can be used to find broken bones, internal bleeding, and cancerous growths.

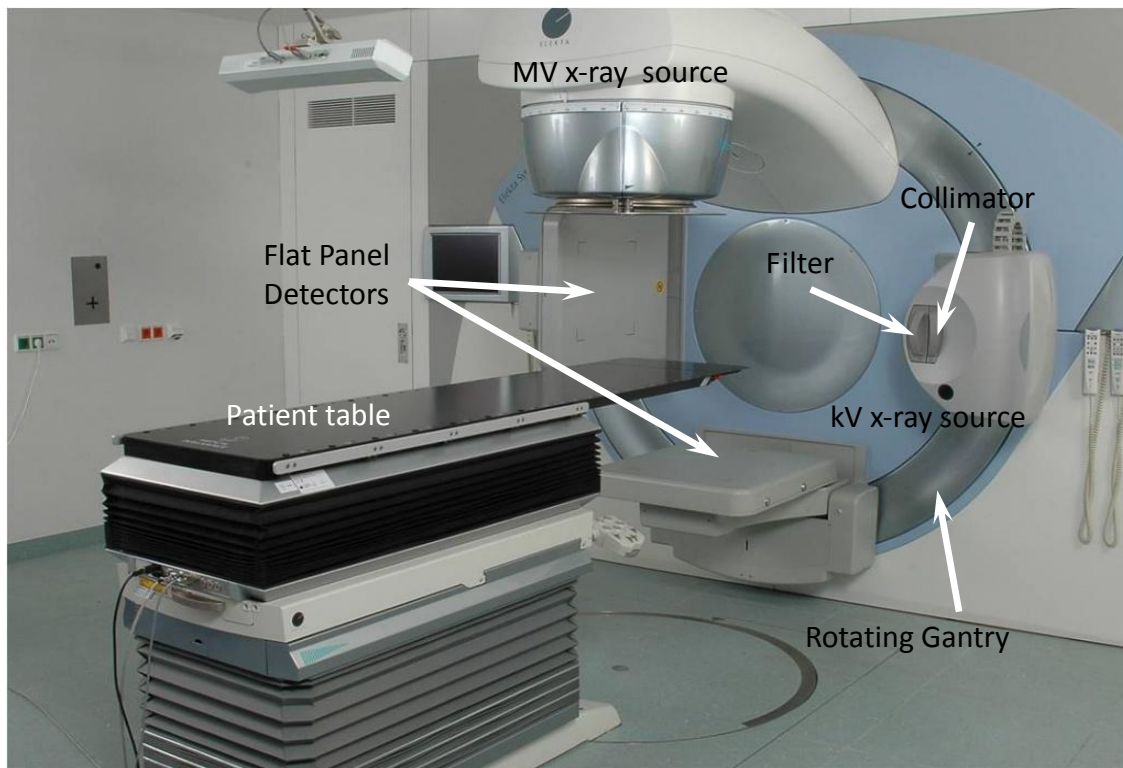


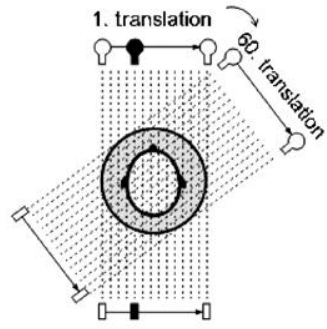
Figure 1. The Elekta Synergy CBCT. The scanner is mounted to the wall of the treatment room. A patient is positioned on the table, and the kV x-ray source and flat panel detector can rotate a full 360° around the patient as it scans.

X-rays have been used to visualize dense objects like bones, but CT scans allow for a full three-dimensional visualization of human tissue, organs, and bones. In this way a CT scan can help visualize the size and precise location of cancerous tumors. With improvements to CT scanning, these devices are being used more and more frequently increasing the need for concern about the effects of cumulative radiation dosage. For this reason efforts have been made to improve the quality of images while reducing the dose received by patients [1, 2, 3, 4, 5].

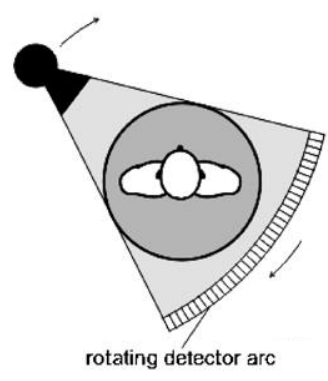
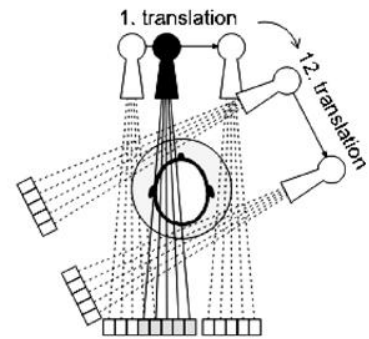
## 1.2 Early CT Scanning

CT scanning was first used in medicine in 1972 after the first scanner [6] was invented by Godfrey Hounsfield in 1967. Allan Cormack is recognized for co-inventing the CT scanner [6] for his theoretical calculations made on the subject. As shown in Figure 2, the history of CT scanners is grouped into four generations of development. The first scanner introduced by Hounsfield was the translate-rotate scanner, which used a pencil beam x-ray source [7]. The image intensifier detector measured the attenuation of the x-ray beam along a single line through a target. The source and detector were translated horizontally along the target, and once the horizontal translation was complete the source and detector were rotated one degree and then translated again. This method of scanning, however revolutionary, was time consuming as a scan could take up to 20 minutes [8]. During this length of time a scan could easily be ruined from patient movement. The second generation of scanners used a similar method of translation and rotation. The difference was the use of a fan beam x-ray source instead of a pencil beam, so multiple detectors arranged in an arc were used instead of the previous single detector. This scanned a larger target area which helped reduce scan time to 5 minutes [6]. The third generation cut down on the amount of time to approximately one minute for a target to be scanned through the use of a cone beam x-ray source [7]. The x-ray source and arc-shaped detector rotated around the target, and translations were no longer necessary since the x-ray beam now covered the area over the z-axis that was previously scanned using translation. The fourth generation was similar to the third with the addition of detectors aligned in a full circle [8] making the x-ray source the only moving part. This innovation did not speed up the average scan time, but limited the number of moving parts during a scan. The fourth generation detectors are more expensive with the large number of detectors, so the third generation detector is more commonly used [7].

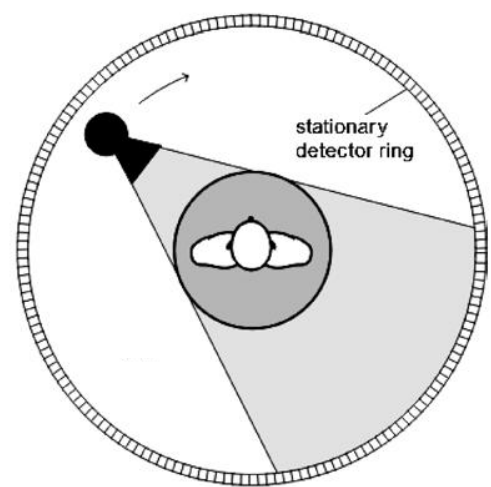
1<sup>st</sup> Generation:  
Translation/Rotation Pencil Beam



2<sup>nd</sup> Generation:  
Translation/Rotation Partial Fan Beam



3<sup>rd</sup> Generation:  
Continuous Rotation Fan Beam



4<sup>th</sup> Generation:  
Continuous Rotation Fan Beam

Figure 2. CT scanner history. The first generations CT scanner used a translate/rotate method with a pencil beam and single detector. The second generation incorporated a fan beam into the translate/rotate method which reduced the amount of time per scan. The third and fourth generations used a cone beam making translation no longer necessary since the cone beam scans in the z-direction already. This figure is from Ref [8].

### 1.3 Cone Beam CT

The newer CT scanners, CBCT scanners, are similar to the third generation of scanners in that the x-ray source and detector rotate with the gantry around the target. CBCT uses a cone shaped array of x-

rays, and a flat panel amorphous-Silicon (a-Si) detector measures beam attenuation through the target, which is used for image reconstruction [9]. As discussed above, the cone beam allows for multiple slices of a target to be scanned at the same time. A CBCT scan can take as little as 10 seconds, which is significantly faster than the original translate and rotate method of the first two generations of scanners [6, 8]. The speed of the scan limits error that may be caused by patient movement.

#### **1.4 Image Quality and Dose**

Attention has more recently been focused on the radiation dose from CT. In 2006, 62 million CT examinations were performed in hospitals in the United States. With continual advancements to CT this number of examinations has been growing at a rate of 15% each year. This means CT contributes to a large percentage of ionizing radiation delivered to the general public [10]. In an effort to decrease dose, CBCT images are analyzed for image quality as a function of the average radiation dosage from the x-ray source. This is important to know as radiation exposure can increase the risk of cancer. A CT scan of the abdomen has an approximate radiation dose of 15 mSv which is equivalent to 5 years of natural background radiation. There would be low risk for an increase in cancer from this dose. However, if a patient needs multiple scans over the course of their treatment the risk of cancer increases. A reduction in the number of white blood cells may occur with 250 – 1000 mSv of dose, limiting the body's ability to fight off diseases. A CT scan never delivers this much dose at one time, but the cumulative dose that a patient may receive can have long term effects [11]. With the improvements to CT scanners radiation dosage has been limited by reducing scan time. CT scanners come with default scan settings from the manufacturer, and these settings could be adjusted to reduce the average scan dose. Mayo et al. ran tests in 1995 to observe image quality as a function of the CT x-ray tube current finding that they could decrease the current by more than half while maintaining adequate image quality [2]. It is necessary to perform similar tests on the CBCT scanners, for the default settings may be higher than necessary.

#### **1.5 CT Images**

CBCT scans were taken with Elekta Synergy (see Figure 1) at Massachusetts General Hospital (MGH) Department of Radiation Oncology in order to analyze them for image quality as a function of radiation dose. Scans were taken of a QA Catphan phantom,

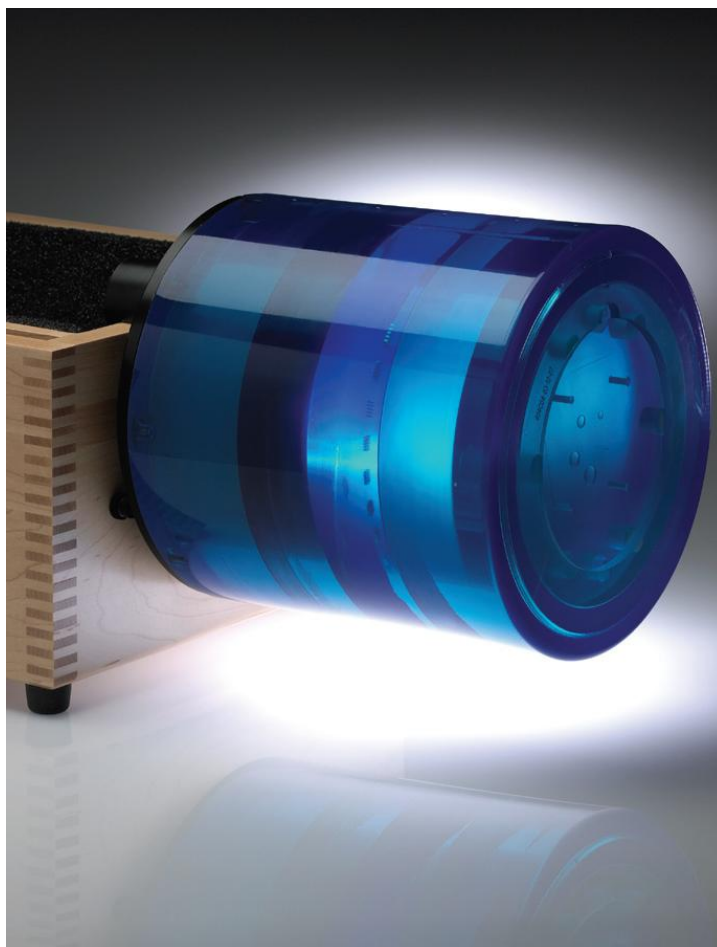


Figure 3. Catphan phantom. The Catphan 500 phantom is approximately 25 cm long with a 16 cm diameter used for QA scans. Each cylindrical section is used to test scanner reconstruction. This figure is from Ref [12].

shown in Figure 3, as well as a human pelvis phantom and a head phantom. The Catphan phantom is a plastic cylinder made with plastics of different densities, made by The Phantom Industries Inc. [12] for the purpose of testing CT image reconstruction quality.

Elekta Synergy is a multi-slice scanner, so each row of detectors in a flat panel detector reconstructs an axial slice of the scanned object. Each slice is reconstructed as a two dimensional, grayscale image. Lighter colored pixels have a higher pixel index and correspond to greater x-ray attenuation, meaning the object is more dense. Likewise, darker pixels mean a lower density, and this is referenced to air such that the pixel index of air is zero as seen in Figure 4.

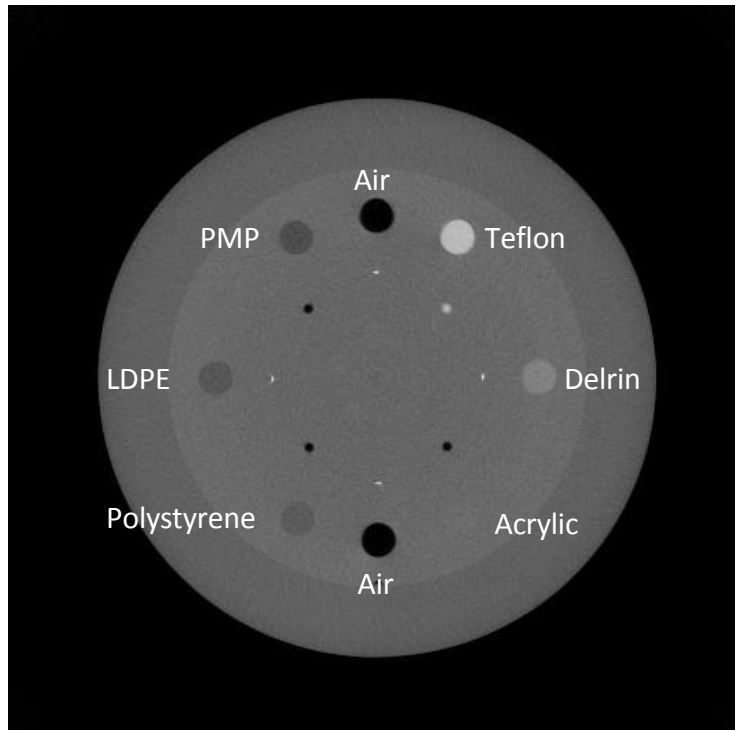


Figure 4. Catphan section 404 scan slice. This is a scanned slice of the Catphan phantom. The different circles are made of different materials.

## *Chapter 2*

### THEORY

#### **2.1 Introduction**

Internal imaging of an object is a complex process involving multiple steps. Up to this point only a basic picture of a CT scanner has been introduced. This scanner is comprised of an x-ray source and detector which rotate around a target. The detector measures the x-ray attenuation which is used for image reconstruction. A three dimensional object is reconstructed using these images. This chapter will explore the steps, from using x-rays to generate a 3D object to analyze, in greater detail.

#### **2.2 The Cone Beam**

Figure 5 shows an Elekta Synergy, which uses an x-ray tube to image a target. The x-ray tube is made up of a filament which is heated and emits electrons. The electrons are then accelerated from a negatively charged cathode to a positively charged rotating tungsten anode. The byproduct of the collision between the electrons and the anode is mostly heat, but also x-rays. The rotating anode helps in cooling.

The final speed of the electrons is dependent upon the potential difference between the anode and cathode. The x-ray beam created by the electron impact is comprised of Bremsstrahlung and characteristic x-ray emission. Bremsstrahlung, or deceleration radiation, occurs when an electron is stopped by the anode. The deceleration of the electron causes it to release electromagnetic energy. Characteristic x-ray emission is when an accelerated electron ejects an electron from the inner valence shell of an atom in the tungsten target. An electron from a higher energy level jumps down to the lower energy level and releases any extra energy. The x-ray tube is contained in a lead casing which absorbs most of the x-ray photons that do not pass through the collimator which forms the cone shaped beam [13]. An x-ray filter is inserted after the collimator to absorb lower energy photons that would be less likely to pass through a target and therefore not benefit image quality [14].

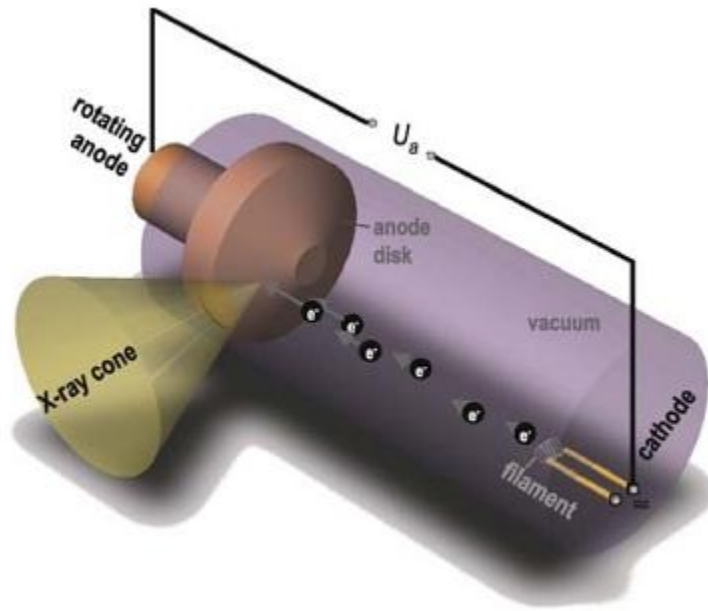


Figure 5. X-ray tube. When there is a potential difference between the anode and cathode, the electrons which are boiled off of the filament, are attracted to the anode. The x-rays produced when the electrons strike the anode are collimated and pass through a window in the side of the tube. This figure is from Ref [13].

### 2.3 Flat Panel Detector

The x-ray photons that are emitted from the kV x-ray source on the gantry are directed at a target and the photon attenuation is measured by an a-Si flat panel detector pictured in Figure 6. The earlier generations of CT scanners used an array of image intensifier detectors, pictured in Figure 7, which use an image intensifier, optics, and a charge coupled device (CCD) television camera to detect x-ray photons. An image intensifier is made up of an input phosphor screen to convert the incoming photon into visible light, a photocathode screen to convert the visible light into an electron which is then accelerated across the image intensifier, due to the electric field, to an output phosphor screen where the electron is converted back into visible light. The light is focused by the lenses and detected by the CCD. Photomultiplier tubes are often used to detect incident photons; however, they cannot measure spatial layouts like a CCD can with its pixel array.

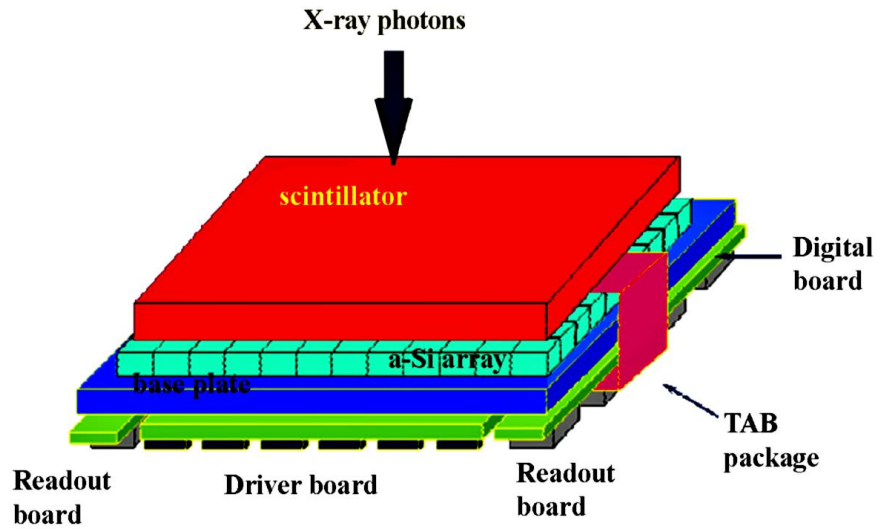


Figure 6. Flat Panel Detector. The amorphous-silicon flat panel detector is made up of a CsI plastic scintillator which converts the x-ray photons into visible light which is then detected by a-Si TFT and read out as an electrical signal. This figure is from Ref [15].

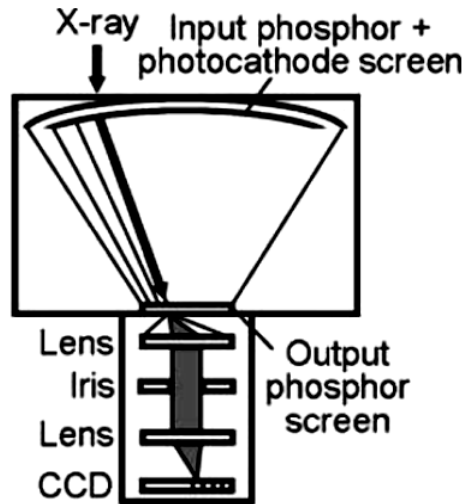


Figure 7. Image Intensifier Detector. The Image Intensifier Detector is the older style CT detector. X-rays are converted to visible light as they hit the input phosphor screen. The visible light converted to an electrons through the photocathode screen which are accelerated across the image intensifier and converted back into visible light by the output phosphor screen. The light is focused through the lenses where it is detected by a CCD. This figure is from Ref [16].

Elekta Synergy uses the newer flat panel detectors which produce images with less noise, or unwanted random variations in image color and brightness, than the image intensifier detectors [16]. A flat panel detector is made up of a cesium iodide (CsI) plastic scintillator screen and an array of a-Si thin film transistors (TFT) where each TFT is attached to its own photodiode as illustrated in Figure 8. Each TFT-photodiode pair makes up a pixel. X-ray photons that pass through the target are converted into visible light by the scintillator since CsI is an excellent absorber of x-rays, the visible light is then read out as an electrical signal through the photodiode. Each TFT acts as a switch such that when a large positive voltage is applied to the gate the switch is closed allowing the pixel to discharge its stored signal electrons through the signal readout to a dataline. The signal is then amplified at the end of the dataline before the voltage is converted to a digital signal [15].

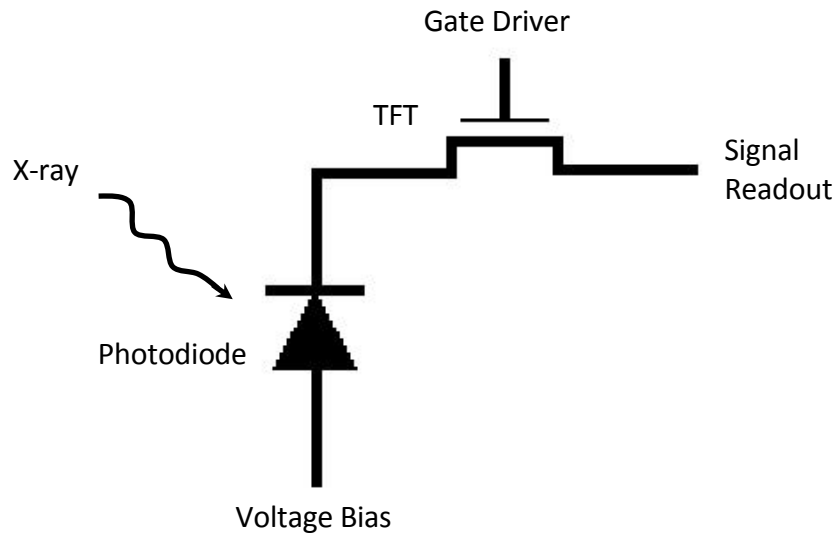


Figure 8. TFT/Photodiode circuit. This is the circuit diagram of a TFT/Photodiode. The light signal from the CsI scintillator is detected by the photodiode and the TFT is a switch which discharges the electrical signal from the photodiode.

## 2.4 Lambert-Beer Law

The flat panel detector measures the decrease in the number of x-ray photons in the beam as a result of absorption or scattering as it passes through a target. This is called attenuation. X-ray beam attenuation, illustrated by Figure 9 and as described by the Lambert-Beer Law [17], has an exponential dependence on the thickness of the material through which the beam passes:

$$I = I_0 e^{-\mu x}. \quad (1)$$

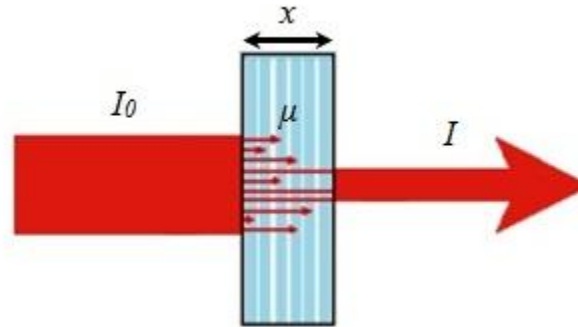


Figure 9. Lambert-Beer Law for homogeneous material of thickness  $x$ .  $I_0$  is the beam intensity before reaching the target,  $I$  is the beam intensity after passing through the target, and  $\mu$  is the attenuation coefficient.

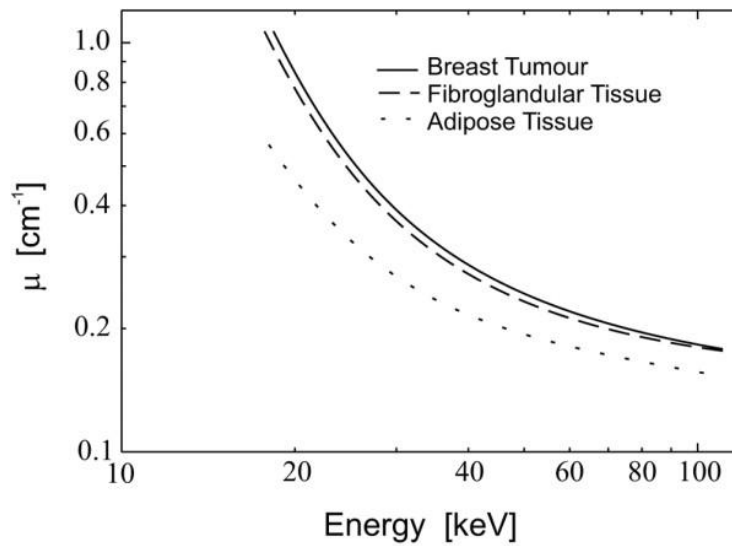


Figure 10. X-ray attenuation plot. Plot of x-ray attenuation coefficient as a function of x-ray energy. The y-axis is x-ray attenuation measured in  $\text{cm}^{-1}$ , and the x-axis is x-ray energy measured in keV. Notice how at higher energies, x-rays penetrate more through materials. This plot also shows that at the same energy different materials have different coefficients of attenuation. The breast tumor is more dense than the surrounding tissue. If this was not the case, then it would be impossible to tell anything apart in a CT scan. This plot is from Ref [18].

The attenuation coefficient is a value that describes how easily a material can be penetrated by the x-rays. As seen in Figure 10, an object with a greater density has a higher attenuation coefficient. If the object is not of uniform density, then the beam attenuation has to be integrated along the beam path [19] as illustrated by Figure 11.

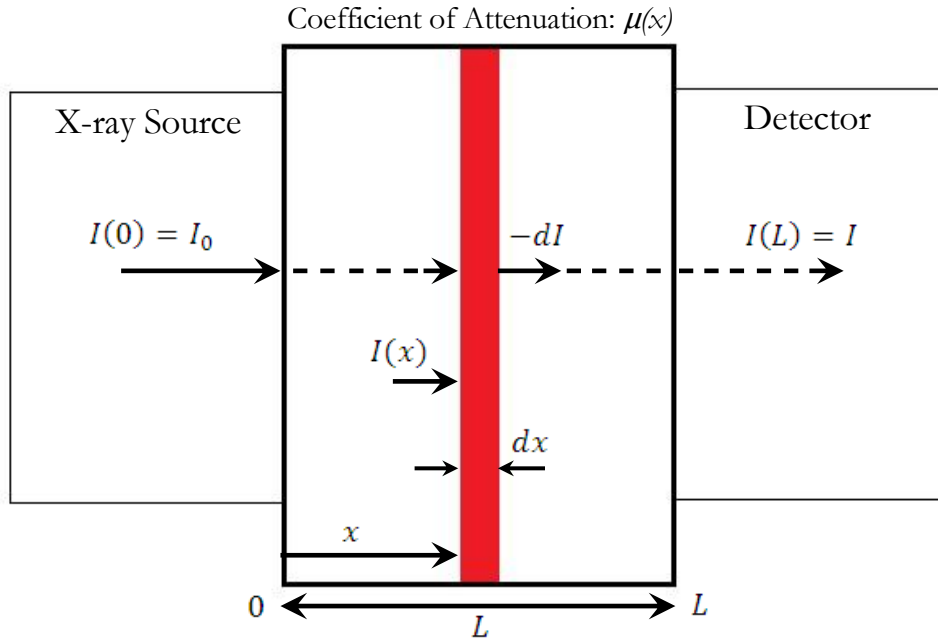


Figure 11. Lambert-Beer Law for inhomogeneous material. Pictorial representation of the Lambert-Beer Law for inhomogeneous materials.  $I_0$  is the number of initial photons,  $-dI$  is the number of photons absorbed by the material of thickness  $dx$ , and  $I$  is the number of detected photons. The attenuation coefficient  $\mu(x)$  is a function of the thickness of the material.

From x-ray attenuation it follows that the number of absorbed photons  $-dI$  in a small slice of the target is proportional to the number of incident photons  $I$  and the thickness of the slice  $dx$ , so

$$-dI \propto I dx. \quad (2)$$

This can be made into an equality where the proportionality constant is the coefficient of attenuation, which is a function of the slice thickness:

$$dI = -\mu(x)I dx. \quad (3)$$

Equation 3 is separable and can be solved for the outgoing beam intensity  $I$  [19].

$$\int_{I_0}^I \frac{dI}{I} = - \int_0^L \mu(x) dx, \quad (4)$$

$$\ln \left( \frac{I}{I_0} \right) = - \int_0^L \mu(x) dx, \quad (5)$$

$$\frac{I}{I_0} = e^{-\int_0^L \mu(x) dx}. \quad (6)$$

Therefore, this derives the Lambert-Beer Law for inhomogeneous materials such as a human.

$$I = I_0 e^{-\int_0^L \mu(x) dx}. \quad (7)$$

This relation says that the beam intensity through a target will decrease exponentially as the target thickness increases [7, 13].

## 2.5 Image Reconstruction

Flat panel detectors observe a 2D projection of the scanned target. Elekta Synergy computer software uses backprojection to recreate the 3D target from the 2D projection. Observe the 2D example in Figure 12 to see how this works. As a beam passes through an object the beam is attenuated and the total attenuation is measured as a function of  $r$ , the orthogonal distance from the origin to the beam, at an angle  $\theta$ , the angle of  $r$  from the x-axis. Since the detector measures the outgoing beam intensity  $I$ , and  $I_0$  is set in the preset settings, then the unknown value in the Lambert-Beer Law is the attenuation coefficient  $\mu$ . Therefore, solve Equation 7 to get

$$R(r, \theta) = \ln \left( \frac{I_0}{I} \right) = \int_a^b \mu(x, y) dl. \quad (8)$$

This line integral is the x-ray transmission along a beam path, where  $R(r, \theta)$  is the projected image as measured by the detector.

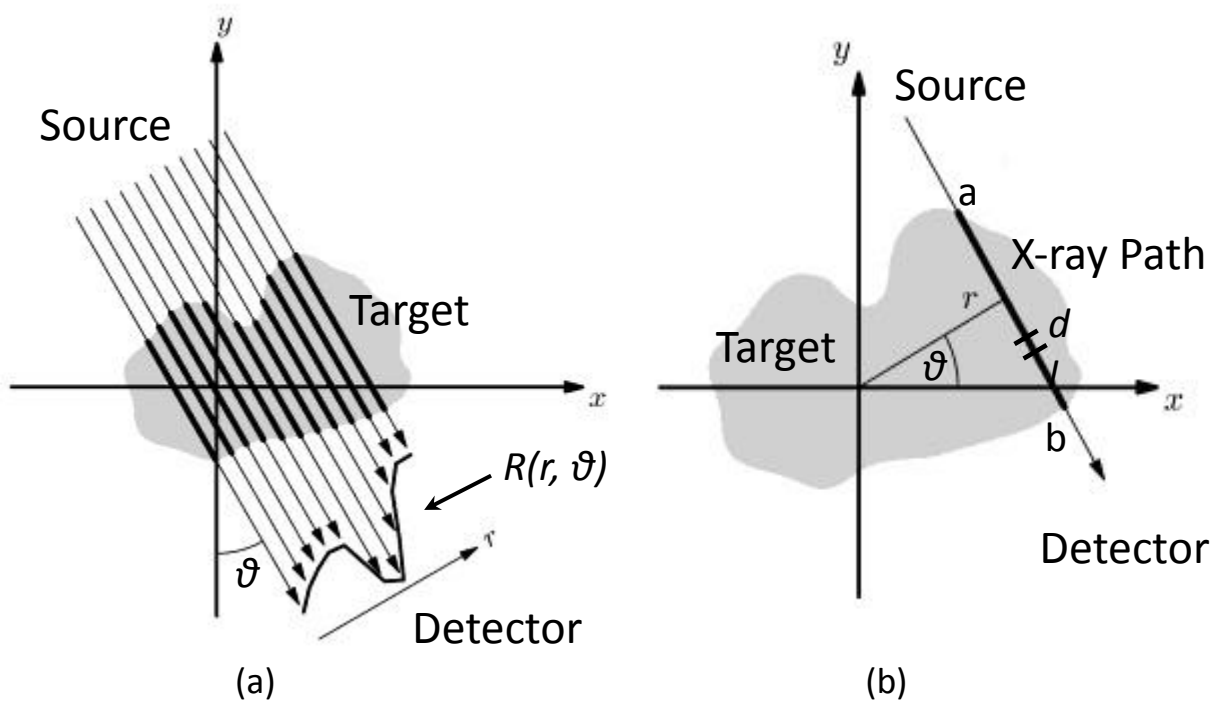


Figure 12. Beam path reconstruction graph. The x-ray beam passes through a (a) target at some angle  $\theta$  and the image  $R(r, \theta)$  is detected, where  $r$  is the orthogonal distance from the origin to beam path. Consider the attenuation of the (b) beam going from  $a$  to  $b$ , which can be broken into tiny lines of length  $dl$ . For a given  $\theta$  make a series of measurements of the attenuation as a function of  $r$ . This figure is from Ref [17].

Now, consider how an image in this case  $\mu(x, y)$  is made up of a collection of pixels. If a pixel has coordinates  $(x, y)$  then the line integral of a line that does not pass through  $(x, y)$  will be zero, and a line that does pass through  $(x, y)$  will have approximately the same value as the attenuation caused by the point. Therefore, the Dirac delta function can be applied to Equation 8 to give

$$R(r, \theta) = \iint \mu(x, y) \delta(x, y) dx dy, \quad (9)$$

where  $\mu(x, y) dx dy$  is the image to be reconstructed. Equation 9 is called the Radon Transformation [17]. The beam path through the point  $(x, y)$  in Figure 12 can be converted into polar coordinates  $(r, \theta)$ . Let the equation of the beam path be  $y = -mx + b$ , then the perpendicular to it through the origin has the equation  $y' = \frac{1}{m}x$ . These two lines intersect when  $y = y'$ . Therefore,

$$-mx + b = \frac{1}{m}x, \text{ so} \quad (10)$$

$$x = \frac{b}{m + \frac{1}{m}}. \quad (11)$$

From the Pythagorean Theorem  $x = r \cos \theta$ , so

$$r \cos \theta = \frac{b}{m + \frac{1}{m}}, \quad (12)$$

and the slope of  $y'$  is  $\tan \theta$ . Therefore,

$$m = \frac{1}{\tan \theta}. \quad (13)$$

Equations 12 and 13 can be used to find

$$b = r \left( \frac{\cos \theta}{\tan \theta} + \sin \theta \right). \quad (14)$$

Now that  $b$  and  $m$  are in terms of  $r$  and  $\theta$ , the equation of the beam path can be written in terms of  $r$  and  $\theta$  using Equations 13 and 14.

$$y = -mx + b = -\frac{1}{\tan\theta}x + r\left(\frac{\cos\theta}{\tan\theta} + \sin\theta\right), \quad (15)$$

$$r = \left(y + \frac{x}{\tan\theta}\right)\left(\frac{\cos\theta}{\tan\theta} + \sin\theta\right)^{-1}. \quad (16)$$

Multiply Equation 16 by  $\frac{\sin\theta}{\sin\theta}$  to get

$$r = (x\cos\theta + y\sin\theta)(\cos^2\theta + \sin^2\theta)^{-1}. \quad (17)$$

Therefore, the equation of the beam path through  $(x, y)$  in polar coordinates is

$$r = x\cos\theta + y\sin\theta. \quad (18)$$

This change of coordinates can now be used to write Equation 9 as

$$R(r, \theta) = \iint \mu(x, y)\delta(r - x\cos\theta - y\sin\theta)dx dy. \quad (19)$$

Inverting Equation 19 and solving for  $\mu(x, y)$  would create a contour plot of the attenuation coefficient which would create an image of the inside of the target. Employ the Fourier Transform

$$f(x, y) = \iint F(r, \theta)e^{2\pi i\theta x}e^{2\pi i\theta y}dr d\theta, \text{ to get} \quad (20)$$

$$\mu(x, y) = \frac{1}{2\pi^2} \iint \frac{1}{r - x\cos\theta - y\sin\theta} \left(\frac{\partial}{\partial r} R(r, \theta)\right) dr d\theta. \quad (21)$$

This is the inverse Radon Transformation [20]. Equation 21 is then used to reconstruct the target. The detector measures the beam attenuation at some  $(r, \theta)$  and then the combination of all the  $\theta$  values for a constant  $r$  value are used to backproject the corresponding  $(x, y)$  point. This is repeated for all  $r$  values until an entire image is reconstructed.



## *Chapter 3*

### IMAGE ANALYSIS

#### **3.1 Introduction**

CBCT images were taken of a quality assurance (QA) Catphan Phantom, head phantom, and pelvis phantom at MGH Department of Radiation Oncology and analyzed using MATLAB for image quality (IQ) as a function of the dose received by the phantom. The goal was to observe whether scan settings could be adjusted such that image quality would be adequate while radiation dosage was decreased. One method of testing IQ was image geometry, where the distances between known points were measured to ensure that the scan reconstructions were accurate. One method of testing IQ was by calculating the contrast-to-noise ratio (CNR) between a region of interest (ROI) on the scan and the background of the image. The image uniformity was tested by plotting the pixel position of a slice of a scan versus the corresponding pixel values. Image uniformity was also tested, using a method similar to that of the CNR algorithm, by comparing four ROI that should have the same density. In most cases the CNR increased with increasing current and decreased as the gantry speed increased. Many of the analysis techniques were taken from Kim et al. [1]. However, the IQ was still good enough even at the lowest current settings and with the gantry speed twice that of the recommended presets. Therefore, it was found that patients can be administered a lower dose and still obtain accurate x-ray images.

#### **3.2 Experimental Procedure**

A CBCT uses a cone shaped array of x-rays to image a patient. The x-ray source is mounted on a gantry arm which then can rotate 360 degrees around a patient. The x-ray detector is opposite the source and rotates with the gantry measuring beam attenuation which is used for backprojection reconstruction. The scanner has different presets that can be used for a scan. The preset scan values were set at Elekta's recommended values. This includes the peak voltage (kVp) ranging from 100 kV to 120 kV, current of the x-ray source pulses ranging from 10 mA to 80 mA, length of the x-ray source pulses ranging from 10 ms to 40 ms, the speed of the gantry, the number of frames to capture, and the start and stop angle of the gantry arc length. Additionally, different presets require different filters and

collimators for the x-ray beam. The main presets are for scans of the head and neck as well as the pelvis and prostate. The dose was then varied by changing values of the presets. To adjust the dose delivered for a selected CBCT scan, the preset values of the gantry speed and the pulse current were varied. As the gantry rotates faster the image resolution decreases, but the radiation dosage also decreases since the scan time is decreased. As the current is increased the image resolution increases, but the dose also increases. These scans were analyzed to observe the image quality as a function of the dose that a patient receives.

The varied preset settings were used to scan phantoms. The three phantoms used were the Catphan 500, head phantom, and pelvis phantom. The Catphan 500 is a cylindrical QA phantom designed to help verify and adjust the settings of a CT scanner. As seen in Figure 3 it is made up of different sections which are used to test image linearity, image uniformity, image density, and image spatial accuracy. Each section of the Catphan is made up of different materials (such as Teflon, Acrylic, and hollow spaces for air) [12] arranged for its specific purpose which will be discussed in the following sections.

The head phantom is a human skull held in an acrylic mold which forms the rest of the head. The pelvis phantom also contained human bones as well as an imitation prostate. The prostate is a plastic of similar density to that of human prostate and the mold is similar to that of human tissue. It is important to run tests on the human phantoms to more carefully observe how the scan settings affect the image quality. Analyzing scans of the Catphan has many benefits in checking for QA, however a scan of a human is not a simple circular picture with known objects in it.

### **3.3 Image Analysis**

The scans were analyzed using MATLAB R2011a. The full code is given in Appendix A. Scans were analyzed for geometrical alignment, density of bone or prostate compared to surrounding tissue, contrast to noise ratio, and image uniformity. A separate algorithm was created for each method of analysis, and then edited depending on the object scanned.

### 3.3.1 Geometrical Alignment

Each MATLAB program was initially created for the Catphan phantom. The Catphan contains four different sections for QA tests. Section 404, as seen in Figure 13, contains four small circles. The three dark ones are air and the light one is Teflon [12]. The different materials appear as different colors because an object's composition is represented by pixel index. A high pixel index represents more dense materials and a low pixel index represents less dense materials where 0 is air.

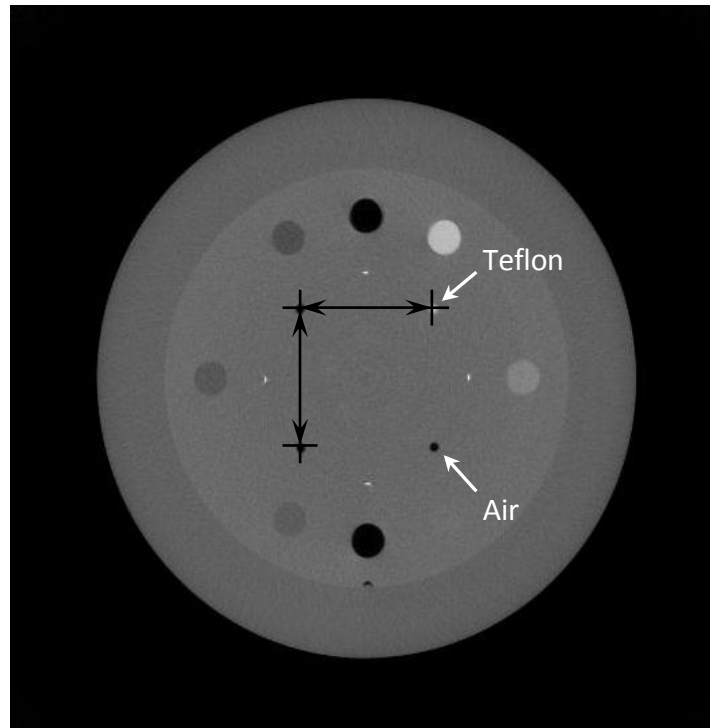


Figure 13. Catphan image alignment. This figure shows the method used to test geometrical alignment. The center of each of the 4 small circles marked by the cross hairs was found using the “centroid” command in MATLAB. The distance between each coordinate was measured to test for linearity.

These circles should create a square with 5 cm edges [12], therefore the diagonal should be 7.07 cm. The algorithm to test this requires the pixel coordinates be input for the general area around the circles. MATLAB then calculates the center of each circle based on the pixel index. The pixel coordinates were then subtracted to find the distance between the centers of the circles.

### 3.3.2 Density

The density of a scanned object was determined by selecting a region of the object and then determining the mean pixel index. The Catphan contains eight cylinders around the outside seen as circles in Figure 4. Each cylinder is made of a different material. To test QA, the pixel indices of the objects were compared to each other. This analysis was used to ensure that the different cylinders were distinguishable from one another.

### 3.3.3 Contrast-to-Noise Ratio

The noise of an image was measured using the standard deviation of the pixel index. This was measured similarly to the density by running the standard deviation function for a selected region of an image. The contrast to noise ratio (CNR) is a way of measuring the image quality by comparing the clarity of region in an image to another separate region, as shown in Figure 14. This is particularly useful when determining how clearly an object is visible in a scan, such as the prostate. The CNR was determined using Equation 22.

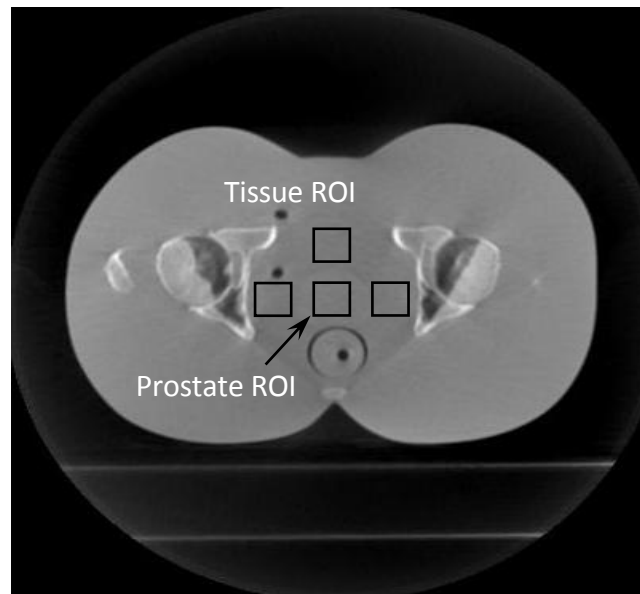


Figure 14. Pelvis phantom CNR. This is a slice from the prostate phantom. The prostate can be visualized by the center ROI. This figure demonstrates the method used to measure the CNR of an image. The mean pixel index of the 3 ROI surrounding the prostate ROI were averaged together to use as a reference ROI with the prostate ROI.

$$CNR = \frac{m_{ROI1} - m_{ROI2}}{\sqrt{s_{ROI1}^2 + s_{ROI2}^2}}, \quad (22)$$

where  $m$  is the mean pixel index and  $s$  is the standard deviation of the pixel index which is a representation of the noise of the ROI.

The ROI were selected based on areas that are important to observe. With the Catphan slice pictured in Figure 13, the ROI's were the circles around the outside. These regions were then compared to a ROI from the very center of the image. Naturally, the greater difference in the density of two objects should mean that the CNR between the two would be greater than two objects of similar density. The ROI from the center was used as reference point, so all regions were compared to it. This was especially important in the analysis of prostate scans, for the prostate is tissue of a similar density to the surrounding tissue. In the case of Figure 14, the prostate has a similar pixel index to the surrounding tissue. When analyzing these scans the reference ROI was the tissue around the prostate, so the CNR helped determine the clarity of an image. As seen in Equation 22, the CNR could be a negative value if the pixel index of  $m_{ROI1}$  is less than  $m_{ROI2}$ . However, the CNR is measured in terms of arbitrary units so negative values simply correspond to lower CNR values.

### 3.3.4 Image Uniformity

Measuring image uniformity was similar to measuring the density of an object in a scan. Four different ROI were selected around the edge of the image and then compared with a ROI from the center, seen in Figure 15. The pixel coordinates of each ROI were selected in MATLAB and then the mean pixel index of each ROI was determined. In a uniform slice of the Catphan, all five ROI's should have the same mean pixel index. This test was used for scans of the head phantom and pelvis phantom as well as the Catphan.

## 3.4 Measuring Radiation

It is important to know how much radiation a patient will receive from a scan. In varying presets the speed of a scan as well as the intensity can be varied, so each preset will give a different dosage to a patient. The dose of a preset was measured by running a scan with a CT dose index (CTDI) phantom, pictured in Figure 16, which has holes in the center of the phantom and at the twelve, three, six, and

nine o'clock positions for an electrometer. A scan was taken with a Keithley 35040 Therapy Dosimeter/Electrometer in each position which measured the ionization produced by the x-rays in

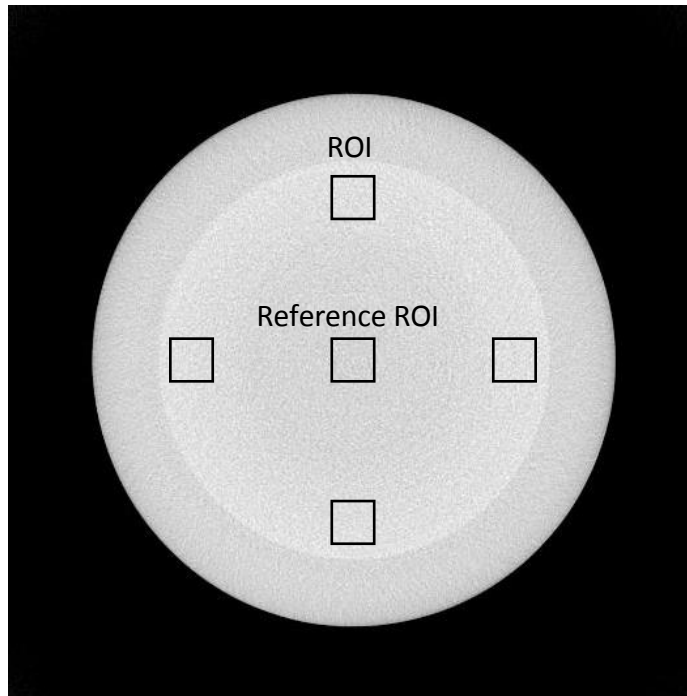


Figure 15. Catphan image uniformity. This is slice from the uniformity section of the Catphan. This section is used to test image uniformity of a reconstructed scan. Each of the 4 outer ROI in the figure were compared with the center reference ROI to test image uniformity.

nanocoulombs (nC), with approximately 1.092 cGy corresponding to 1 nC. The four outer measurements were then averaged together, and the peripheral average is weighted with the center. This is based off of work done by Kim et al. [1].

$$\frac{2}{3}(\text{center}) + \frac{1}{3}(\text{peripheral}) = \text{total}. \quad (23)$$

The total is the weighted CTDI (CTDI<sub>w</sub>) dose was not measured for all presets, but was extrapolated for some. For example, a scan with the gantry rotation speed doubled received half the dose of a normal scan. A linear correlation was likewise assumed between current and dose. With this linear

relation, as presets were adjusted for a scan, the dose could be extrapolated rather than separately measuring the dose, which would take five additional scans.



Figure 16. CTDI Phantom. The electrometer is inserted in the 12 o'clock position on the phantom. A scan is repeated with the electrometer moved to each of the other 3 periphery positions as well as the center. The CTDI<sub>w</sub> is then measured from the 5 scans.

## *Chapter 4*

### RESULTS AND CONCLUSION

#### **4.1 Introduction**

CT scanners have changed and advanced since they were first introduced to the medical world. With every change the patient safety must always be a top priority. Image analysis is one more way to improve CT scans while helping patients by decreasing the dosage. As electron current is increased and the speed of the gantry rotation decreased, the radiation dosage to a patient is increased and it would be expected that image quality would increase as well. After analyzing the various presets for image quality as a function of the CTDI<sub>w</sub>, however, it was observed that the image quality changed little if at all in the CTDI<sub>w</sub> range that was used. The following plots show the observed trend, and how CBCT scans can be given with lower current and with faster gantry speeds while maintaining adequate image quality.

#### **4.2 CBCT Image Quality**

Once the analysis discussed above was carried out on the scans of the various presets, the data were plotted. Plots were made for the image uniformity of a scan as a function of CTDI<sub>w</sub> and for CNR as a function of CTDI<sub>w</sub>. The data tables can be seen in Appendix B.

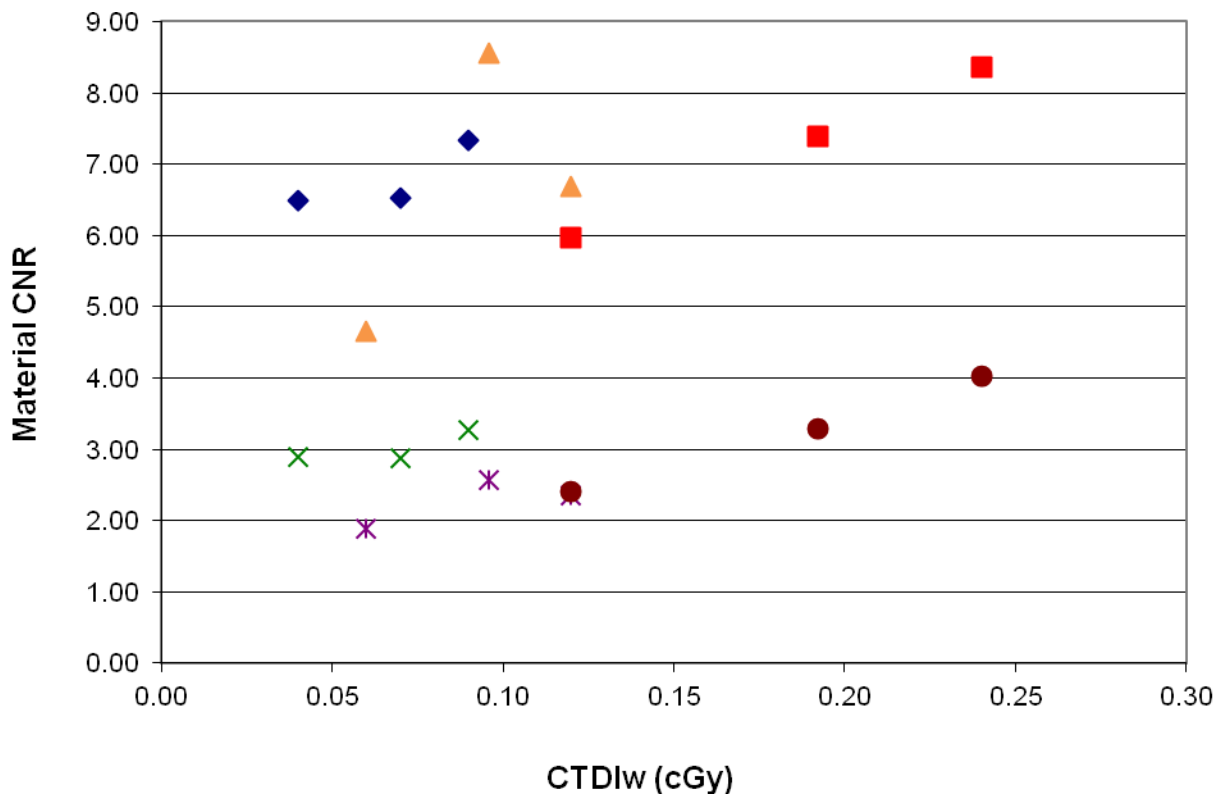


Figure 17. Head and neck image quality plot (Catphan). The y-axis is the CNR, measured in arbitrary units, for the slice of the Catphan seen in Figure 4. The x-axis is the CTDIw (cGy). Measurements were made using the head and neck preset setting with an S20 collimator, an F0 filter (light triangle), and an F1 filter (aluminum) at the normal gantry speed and twice the normal speed. The diamonds and the x's had the F1 filter and ran at twice the normal gantry speed. The triangles and stars had the F0 filter and ran at twice the normal gantry speed. The squares and circles had the F0 filter and ran at the normal gantry speed. The diamonds, triangles, and squares analyzed the Teflon circle on the scan. The x's, stars, and circles analyzed the Delrin circle on the scan. The data has an upward trend as CTDIw increases. However, the increase is rather small such that the scans with the greatest CTDIw do not have a significantly greater CNR.

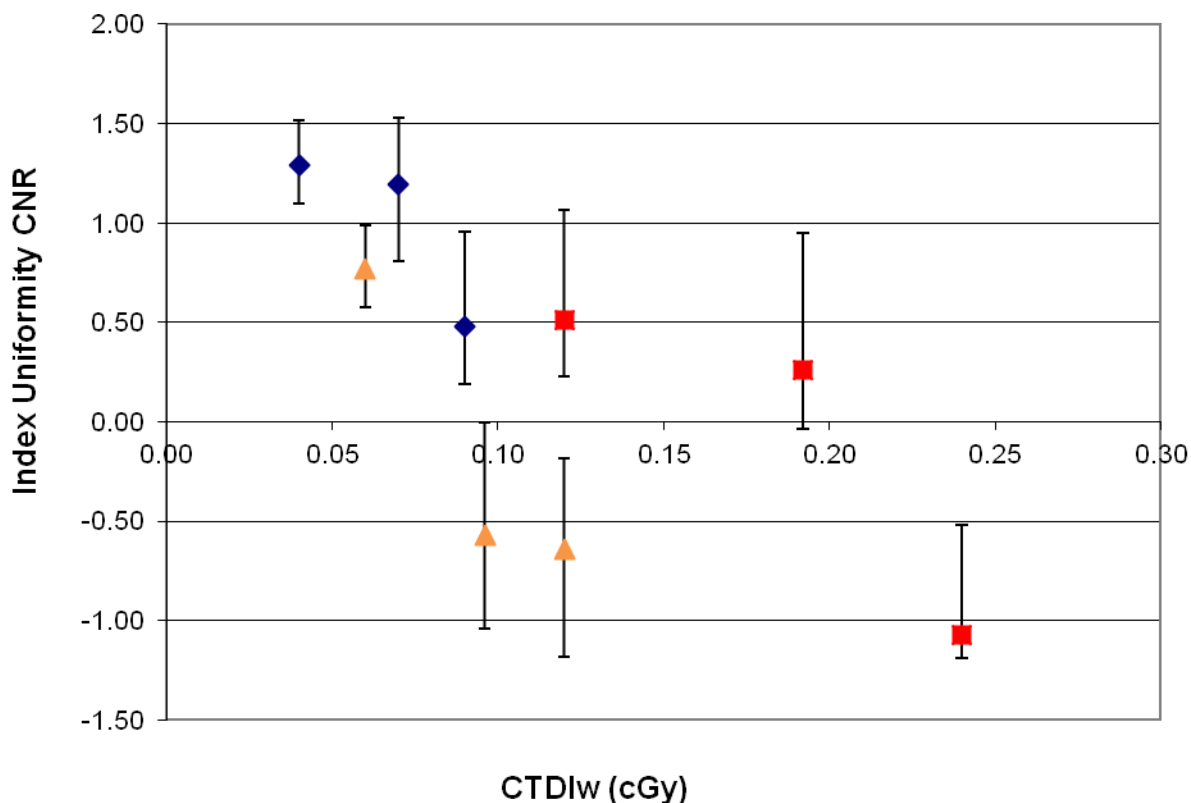


Figure 18. Head and neck uniformity plot (Catphan). The y-axis is the index of uniformity CNR for the slice seen in Figure 15. The x-axis is the CTDIw (cGy). The symbols correspond to the same settings as Figure 17. The mean pixel index of the four outer ROI were averaged together and compared to the pixel index of the center ROI. The error bars show the range of the uniformity when comparing each other ROI to the center ROI. This plot shows that as CTDIw increases the uniformity of the image decreases. Clearly, uniformity would be expected to improve with CTDIw.

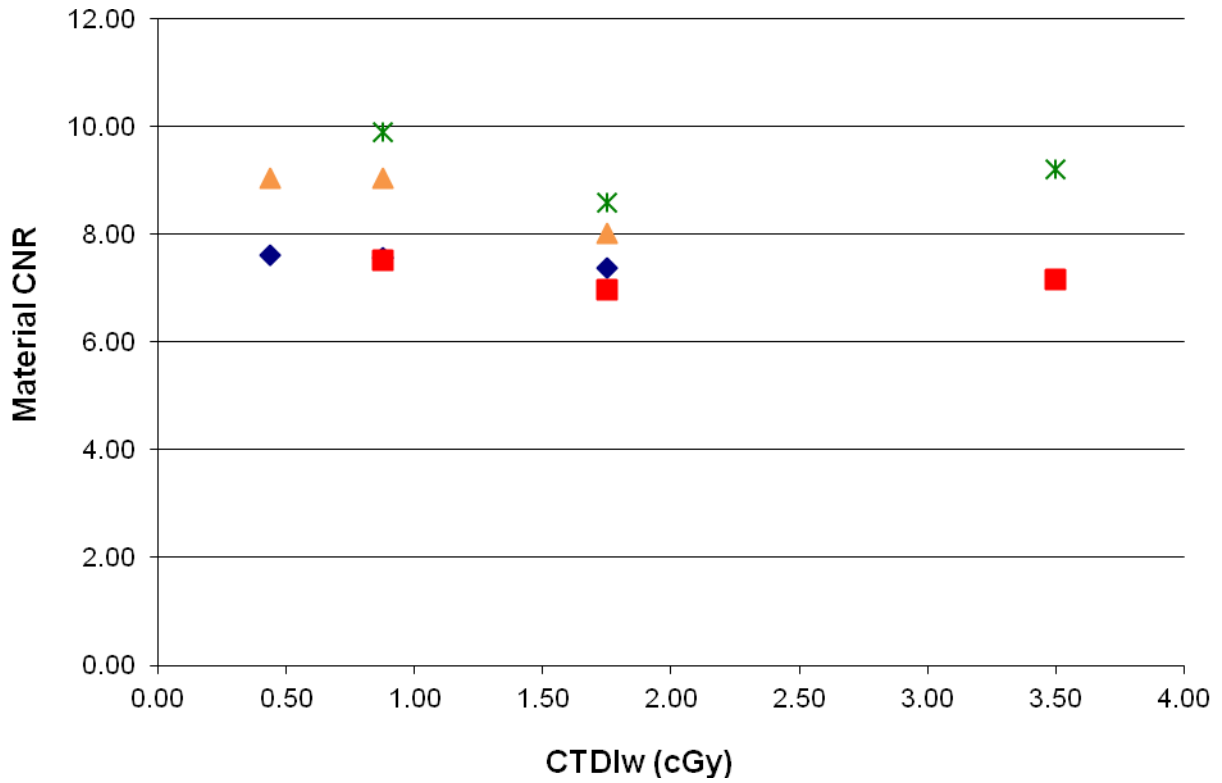


Figure 19. Pelvis image quality (Catphan). The y-axis is the CNR, measured in arbitrary units, for the slice of the Catphan seen in Figure 4. The x-axis is the CTDIw (cGy). Measurements were made using the pelvis preset setting with an M15 collimator and an F1 filter (aluminum) at the normal gantry speed and twice the normal speed. The diamonds and the triangles ran at twice the normal gantry speed. The squares and stars ran at the normal gantry speed. The diamonds and squares analyzed the Teflon circle on the scan. The triangles and stars analyzed the Delrin circle on the scan. Notice how the CNR stays the same as CTDIw increases. Scans should therefore be run at the lowest CTDIw values if there is no change in image quality.

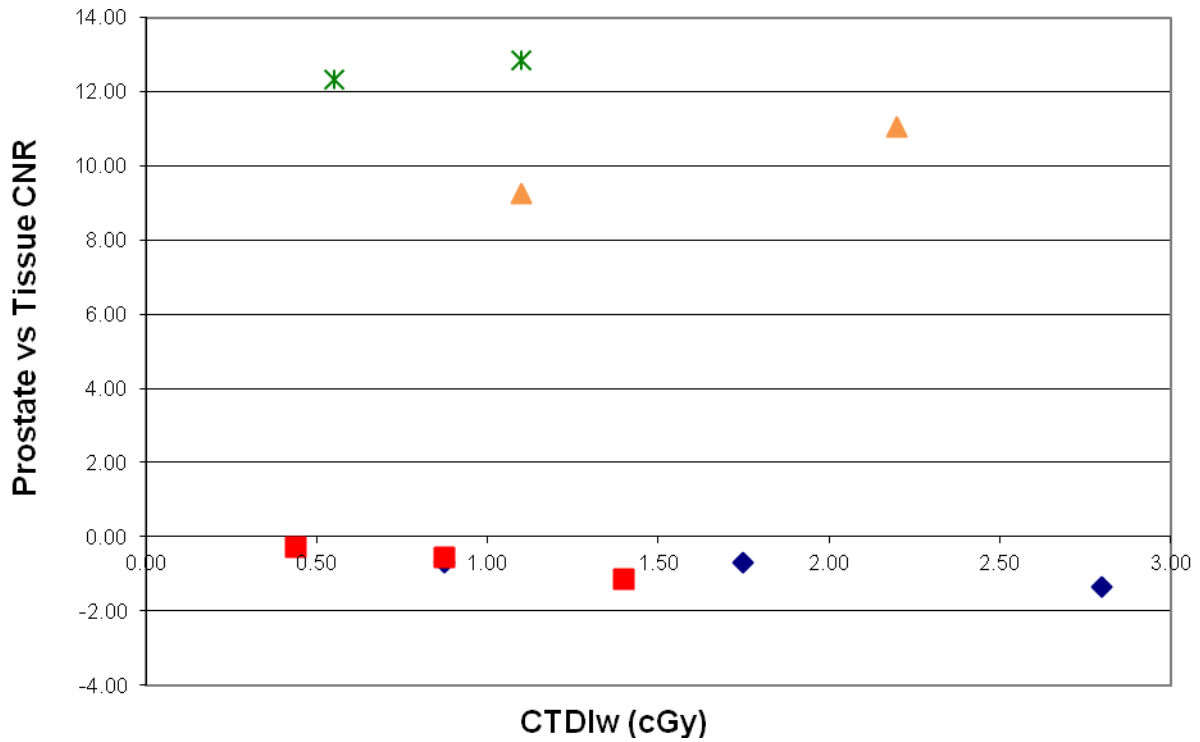


Figure 20. Pelvis image quality (Pelvis Phantom). The y-axis is the CNR between the prostate and the tissue surrounding the prostate (see Figure 14). The x-axis is the CTDIw (cGy). Measurements were made using the pelvis preset setting with an M15 collimator, an L20 collimator, and an F1 filter (aluminum) at the normal gantry speed and twice the normal speed. The squares and the stars ran at twice the normal gantry speed. The diamonds and triangles ran at the normal gantry speed. The diamonds and squares used the M15 collimator. The triangles and stars used the L20 collimator. Again, the CNR stays the same as CTDIw increases. Scans should therefore be run at the lowest CTDIw values if there is no change in image quality. These data points form a horizontal line showing that the CNR does not change with CTDIw.

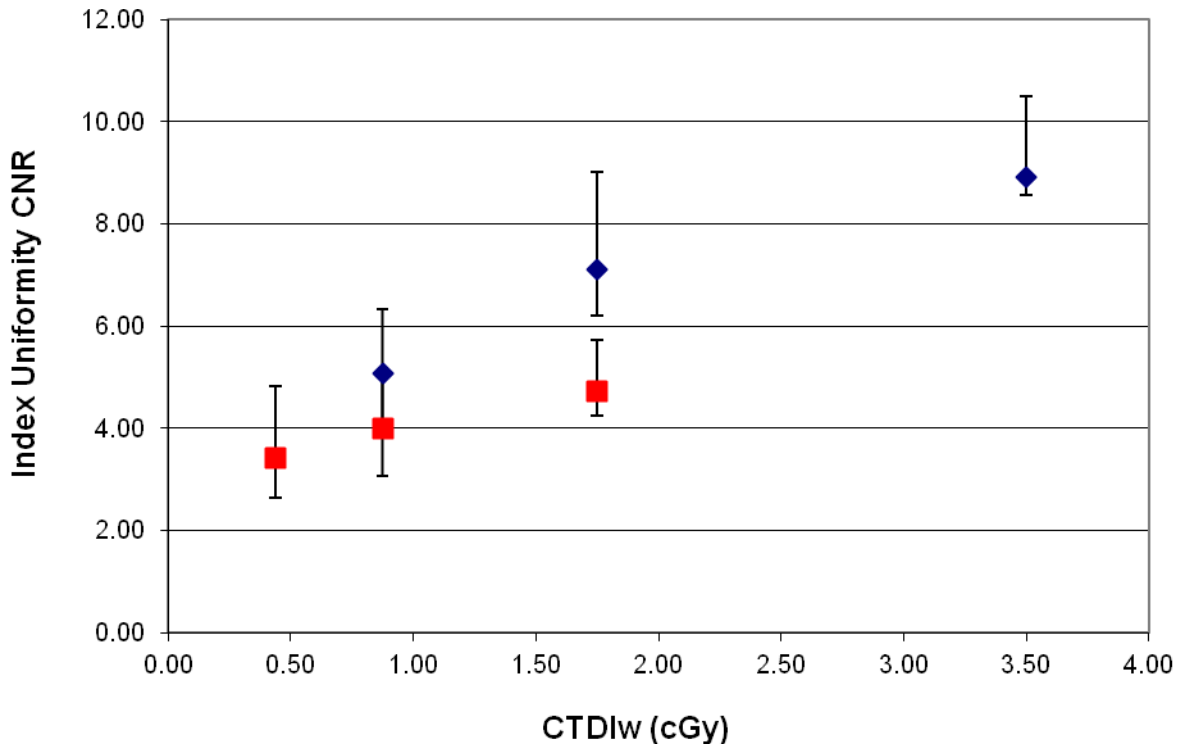


Figure 21. Pelvis uniformity plot (Catphan). The y-axis is the index of uniformity CNR for the slice seen in Figure 15. The x-axis is the CTDIw (cGy). Measurements were made using the pelvis preset setting with an M15 collimator and an F1 filter. The diamonds ran at the normal gantry speed, and the squares ran at double the normal gantry speed. This plot shows that as CTDIw increases the uniformity of the image increases, as would be expected. Through a visual analysis of each scan, the setting with the lowest CTDIw still creates a clear image. The image quality improves at higher CTDIw, but if the images are good at lower levels there is no need to run a scan with the settings as high as the manufacture recommended values.

### 4.3 Discussion

These plots show an overall trend that implies the image quality of a CBCT scan does not change significantly in the CTDIw range that was used for this study. These dose ranges are the typical ranges used in a clinical setting, which means the lower dose scans can be used to create good images. The faster scans can decrease the amount of exposure to radiation by half, and it can also limit the possibility of patient movement during a scan. Elekta's suggested scan settings are higher than necessary for adequate scan reconstruction. These settings can be changed to reduce scan dose to one-

third the suggested setting in in some cases. This is particularly significant for patients who receive numerous scans. For example, during cancer treatment a patient receives many CT scans in order to observe the position and size of a tumor and how it changes over time with treatment. Reductions in CT dose lowers exposure to the general population, and prevents chances of long term effects [10]. CBCT allows for fast 3D patient imaging and dose reduction is significant advantage to add to the list.

#### **4.4 Future Plans**

With the help of this research MGH Department of Radiation Oncology has made changes to some of its CBCT scan preset settings to use lower beam current and to scan at double the gantry speed. Further research is to be carried out is for analyzing image quality for short angle scans, where the x-ray source and detector do not make a full rotation around a target. Clearer CT images are reconstructed when there are more projections, but that does not mean an image cannot be reconstructed with scans from only a few angles. Scan presets can be adjusted for the angles of rotation, so then the same methods of analysis as used for this research could be used to test short angle scan image quality. A short angle scan reduces the amount of time that a patient is scanned, so this is another way to reduce radiation dosage.

## Appendix A

### MATLAB CODE

#### A.1 Coding

This appendix presents the MATLAB code used for image analysis. This particular code was written for images from the Catphan. To use this code for a different phantom, the pixel coordinates of a ROI would simply need to be changed.

#### A.2 Image Density and CNR

This code is used to measure the density of different objects in a scan in terms of pixel index, and it also measures the CNR for the same image.

```
%Contrast to noise ratio and density analysis for Catphan scans
%Calculates the density of each region in terms of pixel index
%Compares the 8 ROIs to the center to observe the contrast to noise ratio

k = 145;    %Enter Slice #
    %Note: Change k = 148 for two scans. See Catphan Excel spreadsheet.

i1 = double(volume_image(158:182,316:340,k));    %Cylinder at 1 o'clock: Teflon
m(1) = mean(mean(i1));    %Calculates the mean index of the above region
s(1) = std(std(i1));    %Calculates the standard deviation of the same region

i3 = double(volume_image(258:282,375:399,k));    %3 o'clock: Delrin
m(2) = mean(mean(i3));
s(2) = std(std(i3));

i5 = double(volume_image(362:384,317:340,k));    %5 o'clock: Acrylic
m(3) = mean(mean(i5));
s(3) = std(std(i5));

i6 = double(volume_image(375:399,259:284,k));    %6 o'clock: Air
m(4) = mean(mean(i6));
s(4) = std(std(i6));

i7 = double(volume_image(359:384,201:225,k));    %7 o'clock: Polystyrene
m(5) = mean(mean(i7));
s(5) = std(std(i7));

i9 = double(volume_image(259:284,142:167,k));    %9 o'clock: LDPE
m(6) = mean(mean(i9));
s(6) = std(std(i9));

i11 = double(volume_image(158:182,200:224,k));    %11 o'clock: PMP
m(7) = mean(mean(i11));
s(7) = std(std(i11));

i12 = double(volume_image(142:167,257:283,k));    %12 o'clock: Air
m(8) = mean(mean(i12));
s(8) = std(std(i12));
```

```

i0 = double(volume_image(258:282,258:282,k));      %Center : Water (Reference)
m(9) = mean(mean(i0));
s(9) = std(std(i0));

cnr(1) = (m(1)-m(9))/sqrt(s(1)^2+s(9)^2);      %Contrast to noise ratio (CNR)
cnr(2) = (m(2)-m(9))/sqrt(s(2)^2+s(9)^2);
cnr(3) = (m(3)-m(9))/sqrt(s(3)^2+s(9)^2);
cnr(4) = (m(4)-m(9))/sqrt(s(4)^2+s(9)^2);
cnr(5) = (m(5)-m(9))/sqrt(s(5)^2+s(9)^2);
cnr(6) = (m(6)-m(9))/sqrt(s(6)^2+s(9)^2);
cnr(7) = (m(7)-m(9))/sqrt(s(7)^2+s(9)^2);
cnr(8) = (m(8)-m(9))/sqrt(s(8)^2+s(9)^2);

```

### A.3 Image Uniformity

This code is used to measure the uniformity of an image. It is nearly identical to the code for measuring CNR. Ideally, the CNR should be zero for a uniform slice since the mean pixel index for two ROI should be the same.

```

%Catphan region of interest (ROI) uniformity test
%Analyzes pieces at 3,6,9 and 12 o'clock and compares them to a region from the
center
%Essentially the same program as cnrdensity.m only this is looking for how similar
regions are instead of how different.

k = 94;      %Enter slice #

i1 = double(volume_image(258:282,388:412,k));      %Coordinates at 3 o'clock
m(1) = mean(mean(i1));
s(1) = std(std(i1));

i2 = double(volume_image(384:408,258:282,k));      %6 o'clock
m(2) = mean(mean(i2));
s(2) = std(std(i2));

i3 = double(volume_image(258:282,132:156,k));      %9 o'clock
m(3) = mean(mean(i3));
s(3) = std(std(i3));

i4 = double(volume_image(128:152,258:282,k));      %12 o'clock
m(4) = mean(mean(i4));
s4 = std(std(i4));

i5 = double(volume_image(258:282,258:282,k));      %Center (Reference)
m(5) = mean(mean(i5));
s(5) = std(std(i5));

roicnr(1) = (m(1)-m(5))/sqrt(s(1)^2+s(5)^2);      %Contrast to Noise Ratio (CNR)
roicnr(2) = (m(2)-m(5))/sqrt(s(2)^2+s(5)^2);
roicnr(3) = (m(3)-m(5))/sqrt(s(3)^2+s(5)^2);
roicnr(4) = (m(4)-m(5))/sqrt(s(4)^2+s(5)^2);

```

### A.4 Image Linearity

This code is used to measure the distance between points on an image. It is specifically designed to test for image reconstruction linearity.

```

%Catphan image geometry/linearity
%Calculates the center of each of the four small inner circles
%Uses the distance formula to calculate the distance between the points

k = 145;    %Enter Slice #

%Inner four cylinders numbered left to right
%Should be 5 cm between each 3 mm cylinder

%ROI pixel coordinates
a = 216;    %x1 left, y1 left, y2 left, x3 left
b = 226;    %x1 right, y1 right, y2 right, x3 right
c = 316;    %x2 left, y3 left, x4 left, y4 left
d = 326;    %x2 right, y3 right, x4 right, y4 right

A = double(volume_image(a:b,a:b,k));    %Top left (Air)
A = -A+2000;    %Inverts the pixels so that in this region air has high index
Circle1 = bwlabel(A>0.8*max(max(A)),8); %Resolution may need to be less than .8
for some H&N scans
Stats = regionprops(Circle1, 'Centroid');
Centroid1 = cat(1,Stats.Centroid);

B = double(volume_image(a:b,c:d,k));    %Top Right (Teflon)
Circle2 = bwlabel(B>0.8*max(max(B)),8);
Stats = regionprops(Circle2, 'Centroid');
Centroid2 = cat(1,Stats.Centroid);

C = double(volume_image(c:d,a:b,k));    %Bottom Left (Air)
C = -C+2000;
Circle3 = bwlabel(C>0.8*max(max(C)),8);
Stats = regionprops(Circle3, 'Centroid');
Centroid3 = cat(1,Stats.Centroid);

D = double(volume_image(c:d,c:d,k));    %Bottom Right (Air)
D = -D+2000;
Circle4 = bwlabel(D>0.8*max(max(D)),8);
Stats = regionprops(Circle4, 'Centroid');
Centroid4 = cat(1,Stats.Centroid);

d12 = (sqrt(((Centroid1(1)+a)-(Centroid2(1)+c))^2+...
((Centroid1(2)+a)-(Centroid2(2)+a))^2))*0.05;    %Distance formula
d24 = (sqrt(((Centroid2(1)+c)-(Centroid4(1)+c))^2+...
((Centroid2(2)+a)-(Centroid4(2)+c))^2))*0.05;    %1 pixel = .05 cm
d34 = (sqrt(((Centroid3(1)+a)-(Centroid4(1)+c))^2+...
((Centroid3(2)+c)-(Centroid4(2)+c))^2))*0.05;
d13 = (sqrt(((Centroid1(1)+a)-(Centroid3(1)+a))^2+...
((Centroid1(2)+a)-(Centroid3(2)+c))^2))*0.05;
%Distance between points given in cm

```

## Appendix B

### PLOTTED DATA

#### B.1 Figure 17 Data

This data was collected by running the image density and CNR program for a slice like Figure 4. It was then plotted in Figure 17.

Technique	X-ray Filter	Beam Current (mA)	Exposure Time (ms)	CTDIw (cGy)	CNR	
					1 o'clock	3 o'clock
					Teflon	Delrin
H&NS20	F0	10.0	10.0	0.12	5.98	2.41
H&NS20	F0	16.0	10.0	0.19	7.39	3.29
H&NS20	F0	20.0	10.0	0.24	8.37	4.03
FastH&NS20	F0	10.0	10.0	0.06	4.65	1.89
FastH&NS20	F0	16.0	10.0	0.10	8.55	2.57
FastH&NS20	F0	20.0	10.0	0.12	6.68	2.36
FastH&NS20	F1	10.0	10.0	0.04	6.49	2.90
FastH&NS20	F1	16.0	10.0	0.07	6.52	2.87
FastH&NS20	F1	20.0	10.0	0.09	7.34	3.27

#### B.2 Figure 18 Data

This data was collected by running the image uniformity program for a slice like Figure 15. It was then plotted in Figure 18.

Technique	X-ray Filter	Beam Current (mA)	Exposure Time (ms)	CTDIw (cGy)	CNR		
					Average	Lower Limit	Upper Limit
H&NS20	F0	10.0	10.0	0.12	0.51	0.29	0.55
H&NS20	F0	16.0	10.0	0.19	0.26	0.30	0.69
H&NS20	F0	20.0	10.0	0.24	-1.07	0.12	0.55
FastH&NS20	F0	10.0	10.0	0.06	0.77	0.20	0.21
FastH&NS20	F0	16.0	10.0	0.10	-0.57	0.47	0.56

FastH&NS20	F0	20.0	10.0	0.12	-0.64	0.54	0.46
FastH&NS20	F1	10.0	10.0	0.04	1.29	0.19	0.23
FastH&NS20	F1	16.0	10.0	0.07	1.20	0.39	0.33
FastH&NS20	F1	20.0	10.0	0.09	0.48	0.29	0.48

### B.3 Figure 19 Data

This data was collected by running the image density and CNR program for a slice like Figure 4. It was then plotted in Figure 19.

Technique	X-ray Filter	Beam Current (mA)	Exposure Time (ms)	CTDIw (cGy)	CNR	
					1 o'clock	3 o'clock
					Teflon	Delrin
PelvisM15	F1	20.0	40.0	0.88	7.51	9.89
PelvisM15	F1	40.0	40.0	1.75	6.96	8.57
PelvisM15	F1	80.0	40.0	3.50	7.16	9.19
FastPelvisM15	F1	20.0	40.0	0.44	7.61	9.02
FastPelvisM15	F1	40.0	40.0	0.88	7.55	9.03
FastPelvisM15	F1	80.0	40.0	1.75	7.37	8.01

### B.4 Figure 20 Data

This data was collected by running the image density and CNR program for a slice like Figure 14. It was then plotted in Figure 20.

Technique	X-ray Filter	Beam Current (mA)	Exposure Time (ms)	CTDIw (cGy)	Speed	Frames	kVp	mAs/projection
PelvisM15	F1	20.00	40.00	0.88	180	660	120	0.80
PelvisM15	F1	40.00	40.00	1.75	180	660	120	1.60
PelvisM15	F1	64.00	40.00	2.80	180	660	120	2.56
FastPelvisM15	F1	20.00	40.00	0.44	360	330	120	0.80
FastPelvisM15	F1	40.00	40.00	0.88	360	330	120	1.60
FastPelvisM15	F1	64.00	40.00	1.40	360	330	120	2.56
PelvisL20	F1	32.00	40.00	1.10	180	660	120	1.28
PelvisL20	F1	64.00	40.00	2.20	180	660	120	2.56
FastPelvisL20	F1	32.00	40.00	0.55	360	330	120	1.28
FastPelvisL20	F1	64.00	40.00	1.10	360	330	120	2.56

### B.5 Figure 21 Data

This data was collected by running the image uniformity program for a slice like Figure 15. It was then plotted in Figure 21.

Technique	X-ray Filter	Beam Current (mA)	Exposure Time (ms)	CTDIw (cGy)	CNR		
					Average	Lower Limit	Upper Limit
PelvisM15	F1	20.0	40.0	0.88	5.07	1.04	1.28
PelvisM15	F1	40.0	40.0	1.75	7.10	0.89	1.92
PelvisM15	F1	80.0	40.0	3.50	8.93	0.35	1.57
FastPelvisM15	F1	20.0	40.0	0.44	3.41	0.76	1.41
FastPelvisM15	F1	40.0	40.0	0.88	3.99	0.93	1.17
FastPelvisM15	F1	80.0	40.0	1.75	4.73	0.49	1.00

## REFERENCES

- [1] S. Kim *et. al.*, *Med. Phys.* **37**, 3648 (2010).
- [2] J. R. Mayo *et. al.*, *AJR Am. J. Radiol.* **164**, 603 (1995).
- [3] K. Bacher *et. al.*, *AJR Am. J. Radiol.* **181**, 923 (2003).
- [4] A. Amer *et. al.*, *Br. J. Radiol.* **80**, 476 (2007).
- [5] M. K. Islam *et. al.*, *Med. Phys.* **33**, 1573 (2006).
- [6] W. A. Kalender, *Phys. Med. Biol.* **51**, 29 (2006).
- [7] P. Sukovic, AADMRT Newsletter, “Cone Beam Computed Tomography in Dentomaxillofacial Imaging,” (2004).
- [8] L. W. Goldman, *J. Nucl. Med. Technol.* **35**, 115 (2007).
- [9] J. Lehmann *et. al.*, *Med. Phys.* **8**, 21 (2007).
- [10] C. H. McCollough *et. al.*, *AAPM* **96**, 1 (2008).
- [11] A. Bruner *et. al.*, *Bayl. Univ. Med. Cent.* **22**, 119 (2009).
- [12] D. J. Goodenough, “Catphan 500 and 600 Manual,” <http://www.phantomlab.com/library/pdf/catphan500-600manual.pdf>.
- [13] T. M. Buzug, *Computed Tomography: From Photon Statistics to Modern Cone-Beam CT*, (Springer, Germany, 2008).
- [14] N. Mail *et. al.*, *Med. Phys.* **36**, 22 (2009).
- [15] Varian Medical Systems, “Paxscan,” <http://www.varian.com/media/xray/products/pdf/Flat%20Panel%20Xray%20Imaging%2011-11-04.pdf>.
- [16] R. Baba, K. Ueda, and M. Okabe, *Br. J. Radiology*, **33**, 285 (2004).
- [17] M. Figl and J. Hummel, *Applied Medical Image Processing: A Basic Course* (Taylor & Francis, Boca Raton, FL, 2011), pp. 319-349.

[18] M. J. Yaffe, *Breast Cancer Research*, **10**, 209 (2008).

[19] A. C. Miracle and S. K. Mukherji, *Am. J. Neuro.* **30**, 1088 (2009).

[20] L. A. Feldkamp *et. al.*, *J. Opt. Soc. Am. A.* **1**, 612 (1984).